Volume 17
Number 27
21 July 2025
Pages 16043-16546

Nanoscale

rsc.li/nanoscale

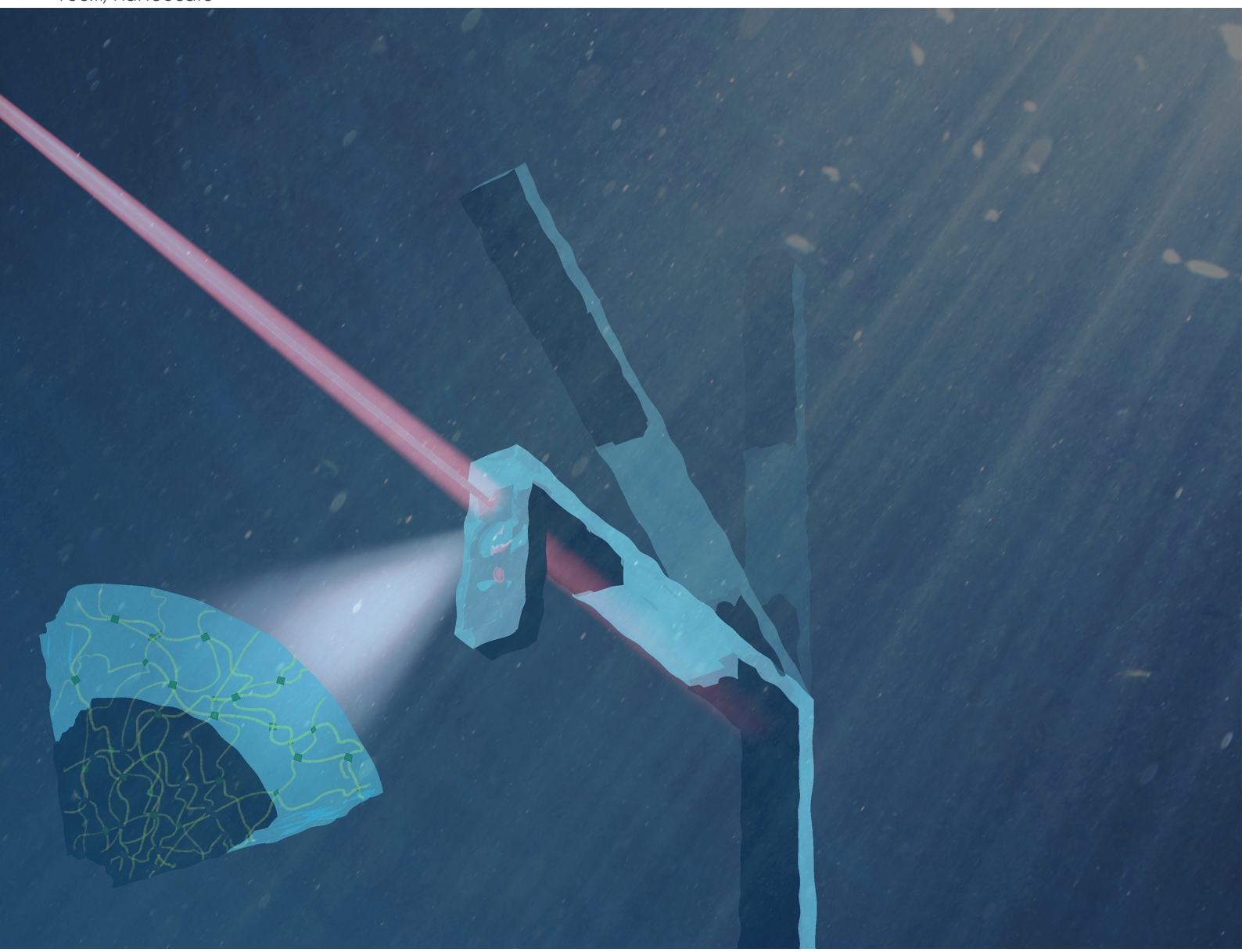

ISSN 2040-3372

ROYAL SOCIETY OF CHEMISTRY

PAPER
Alan C. H. Tsang *et al.*
Self-regulated photoresponsive heterogeneous PNIPAM hydrogel actuators

NCNST

Nanoscale

PAPER

View Article Online
View Journal | View Issue

Cite this: *Nanoscale*, 2025, **17**, 16230

Self-regulated photoresponsive heterogeneous PNIPAM hydrogel actuators†

Jingxuan Li,‡ Jiaqi Miao‡ and Alan C. H. Tsang *

Received 13th December 2024,
Accepted 23rd May 2025

DOI: 10.1039/d4nr05257a

rsc.li/nanoscale

Self-regulated actuators harness material intelligence to enable complex deformations and dynamics, representing a significant advancement in automated soft robotics. However, investigations on self-regulated soft actuators, particularly those using simplified actuation modules, such as a unidirectional light beam, remain limited. Here, we present a design paradigm for self-regulated actuators based on poly(*N*-isopropylacrylamide) (PNIPAM) heterogeneous hydrogels, where self-regulated deformations are actuated using a fixed near-infrared laser. By utilizing the different responsiveness of PNIPAM hydrogels and those integrated with reduced graphene oxide (rGO), we have developed three heterogeneous hydrogel configurations: up–down, side-by-side, and hybrid types. These designs enable complex biomimetic deformations in soft hydrogel actuators, resembling a bending finger or a flexible industrial manipulator, all actuated using a single fixed-laser source. These proposed heterogeneous designs and actuation strategies leverage material intelligence to create soft actuators with enhanced autonomy, paving the way for soft automation, adaptive systems, and biomedical applications.

Introduction

Soft actuators, inspired by biological organisms' movement and functionalities, are designed to emulate their flexibility and adaptability.[1–3] Researchers have developed soft actuators capable of navigating challenging environments, performing delicate tasks, and interacting safely with humans.[4–6] The design of soft actuators emphasizes their ability to deform, stretch, and contract[7–10] under diverse external field actuation,[11–13] *e.g.*, light, magnetic, electric, *etc*. Owing to the flexibility of soft materials, these actuators can carry out intricate movements and functions without the need for extra rigid components, offering significant advantages in miniaturization,[14,15] particularly for applications in confined spaces and biomedical fields.[16–18]

Poly(*N*-isopropylacrylamide) (PNIPAM) hydrogels have received significant attention in soft robotics due to their unique thermoresponsive properties.[19,20] At temperatures below their lower critical solution temperature (LCST) of approximately 32 °C, PNIPAM hydrogels exhibit a swollen, hydrophilic state, allowing for high water content and flexibility. Conversely, upon heating above the LCST, these hydrogels undergo a dramatic volume phase transition, becoming hydrophobic and shrinking significantly. This reversible response to temperature changes enables PNIPAM-based materials to mimic biological systems and perform complex deformations.[21] Furthermore, the incorporation of photothermal agents into hydrogels enables them to respond to light stimuli, *e.g.*, near-infrared (NIR) lasers, resulting in rapid

Department of Mechanical Engineering, The University of Hong Kong, Pokfulam, Hong Kong, China. E-mail: alancht@hku.hk; Tel: +852 3917 1505

†Electronic supplementary information (ESI) available. See DOI: https://doi.org/10.1039/d4nr05257a

‡These authors contributed equally to this work.

Alan C. H. Tsang

Alan C. H. Tsang is an assistant professor of mechanical engineering at the University of Hong Kong (HKU). He received his B. Eng. and M.Phil. degrees in mechanical engineering from HKU and Ph.D. in mechanical engineering from the University of Southern California. He then continued his research as a postdoctoral research fellow at Stanford University and the University of Arizona before he joined HKU. His research group employed theoretical tools of applied mathematics, computer simulations, machine learning and different experimental tools to investigate fundamental and application problems in fluid mechanics and biophysics. His research interests include active matter, microfluidics, micro-swimmers and biological adaptation.

deformations, including but not limited to bending,[22,23] crawling,[24] and swimming.[25] This makes photoresponsive hydrogels ideal for applications in soft robotics, drug delivery, and tissue engineering.[26–30]

Despite great advances, hydrogel actuators are typically designed to follow specific motion modes under given external fields, forbidding their applications for complex maneuver tasks that require adaptive switching between deformation modes. Recently, self-regulated soft actuators have shown adaptive movements by employing novel actuation strategies along with unique designs.[31–35] In particular, self-regulated actuators driven by light have demonstrated remarkable oscillatory dynamics *via* self-shadowing effects.[36,37] However, a complex actuation method (*e.g.*, introducing multiple laser illuminations[38]) is required to achieve complex multi-bending movement or mode switching. An important next stage for intelligent soft actuators is to develop self-regulated deformations under simplified actuation conditions (*e.g.*, a fixed single-laser source).

In this work, we present PNIPAM-based soft heterogeneous hydrogel actuators that generate self-regulated deformations when stimulated by a fixed NIR laser. The heterogeneous PNIPAM hydrogel actuators comprise two portions made from pure PNIPAM hydrogels and hydrogels embedded with reduced graphene oxide (rGO). The difference in the responsiveness of these two hydrogel portions forms the basis for light-driven deformation (Fig. 1a). Utilizing these two building blocks (denoted as 0 for the PNIPAM hydrogel and 1 for the PNIPAM/rGO hydrogel), as shown in Fig. 1b-i, we introduce three heterogeneous configurations: up–down, side-by-side and hybrid types (Fig. 1b-ii). These heterogeneous designs enable hydrogel actuators to achieve self-regulated multimodal deformations (Fig. 1c), facilitating complex movements akin to those of finger bending and flexible industrial manipulators. All actuation controls are executed through a single fixed NIR laser setup, which significantly simplifies the control module and enhances operational efficiency. These advantages position the self-regulated heterogeneous hydrogel actuator as a promising candidate for future applications in soft automation, adaptive systems, and biomedical devices.[39–42]

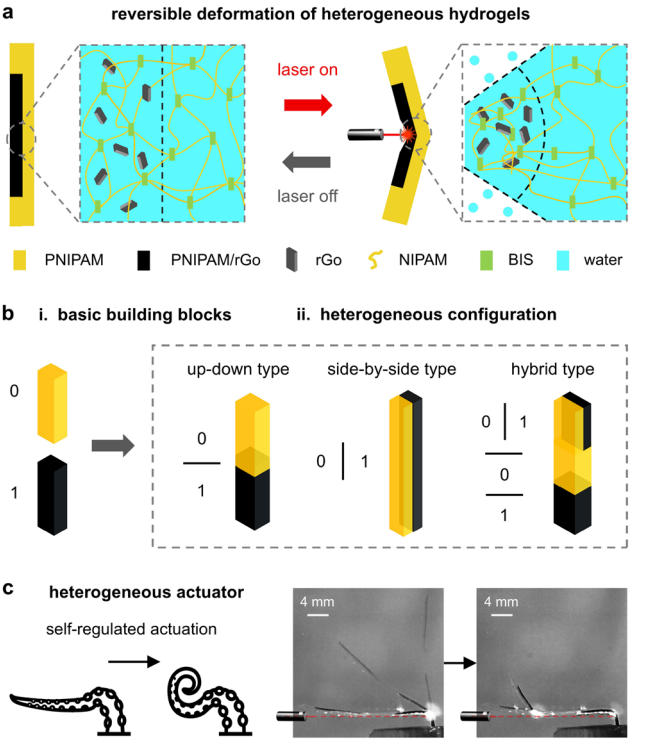

Fig. 1 Illustration of the design concept of self-regulated heterogeneous hydrogel actuators. (a) NIR-driven reversible deformation of heterogeneous hydrogels. (b) (i) Two basic building blocks: PNIPAM hydrogel (0) and PNIPAM/rGo hydrogel (1); (ii) three heterogeneous configurations: up–down, side-by-side and hybrid types. (c) Heterogeneous soft hydrogel actuators featuring self-regulated deformations under a fixed NIR laser.

Results and discussion

Fabrication and characterization of PNIPAM-based hydrogels

Here, we introduce *in situ* reduced graphene oxide (rGO) as a photothermal agent to create PNIPAM/rGO hydrogels, adding heterogeneity to the PNIPAM hydrogel. We synthesize PNIPAM and PNIPAM/GO hydrogels by curing precursors under ultraviolet (UV) light, and obtain PNIPAM/rGO hydrogels by the ascorbic acid reduction method (Experimental section and Fig. S1, ESI†). Scanning electron microscopy (SEM) images show that both PNIPAM and PNIPAM/rGO hydrogels possess similar loose porous networks (Fig. 2a and the Experimental section), which ensure their rapid response and recovery. We recorded the Fourier transform infrared (FTIR) spectra of PNIPAM and PNIPAM/rGO, as shown in Fig. 2b (Experimental section). The characteristic absorption bands of PNIPAM are indicated by peaks located at 3279 cm^{-1} (secondary amide N–H stretching), 1622 cm^{-1} (amide I, C=O), and 1541 cm^{-1} (amide II, N–H).[43] In comparison, the spectrum of PNIPAM/rGO exhibits noticeable shifts to new characteristic absorption bands at approximately 3285 cm^{-1}, 1631 cm^{-1}, and 1534 cm^{-1}, confirming the interaction between PNIPAM and rGO in the hydrogels.

Fig. 2c presents the tensile strength test results of PNIPAM and PNIPAM/rGO hydrogels (Experimental section). The PNIPAM hydrogels have inherently poor mechanical properties.[44] The doping of rGO enhances mechanical properties due to the interweaving of graphene's two-dimensional grid structure with the hydrogel during cross-linking.

In Fig. 2d, we evaluate the swelling properties of PNIPAM and PNIPAM/rGO hydrogels with different amounts of cross-linking agent (BIS) by calculating their mass-change ratio R_M and volume-expansion ratio R_V (Experimental section). As the concentration of BIS increases, the density of the cross-linked network also increases, resulting in a gradual decrease in the equilibrium water content of PNIPAM and PNIPAM/rGO hydrogels.

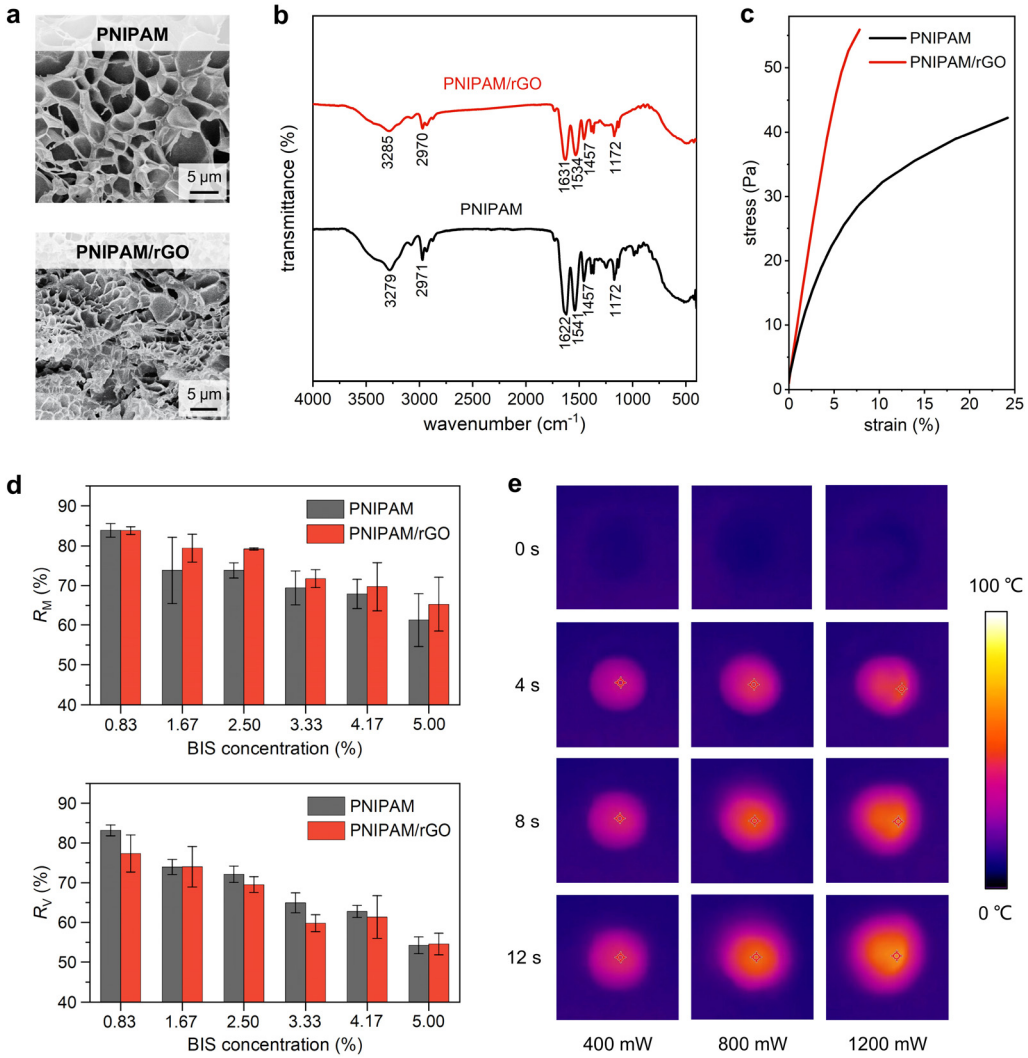

Fig. 2 Characterization of PNIPAM-based hydrogels. (a) SEM images of PNIPAM and PNIPAM/rGO hydrogels. (b) FTIR spectra of PNIPAM and PNIPAM/rGO hydrogels. (c) Tensile stress–strain curves of PNIPAM and PNIPAM/rGO hydrogels. (d) Volume-expansion ratio and mass-change ratio of PNIPAM and PNIPAM/rGO hydrogels at different BIS concentrations (mean ± SD for three samples in each case). (e) Photothermal response of PNIPAM/rGO hydrogels (GO: 1.5 g mL^{-1}) at varying laser intensities (400 mW, 800 mW, and 1200 mW) over time.

We also compare the photothermal conversion efficiency of PNIPAM/rGO hydrogel samples with varying contents of photothermal agent (Experimental section and Fig. S2 and S3, ESI†). We record the photothermal response of the hydrogels with optimal graphene oxide content (1.5 mg mL^{-1}) at different NIR laser intensities over time (Fig. 2e). The photothermal conversion rate increases with the intensity of the laser. The rapid conversion allows the temperature of the PNIPAM/rGO hydrogel to exceed its LCST quickly, leading to localized contraction within heterogeneous hydrogels and thereby enabling various deformations.

The UV-curing process ensures the rapid fabrication of PNIPAM and PNIPAM/rGO hydrogels. Due to their shared base materials, these components adhere well during sequential curing, allowing for the assembly of various building blocks, as shown in Fig. 1b-ii. We use a mold-assisted method to create hydrogels of different shapes. The low flowability of the high-viscosity PNIPAM/GO precursor (Fig. S4, ESI†) supports multiple curing rounds (Experimental section). The hybrid-type heterogeneous hydrogels constructed in this manner have the potential to be developed into diverse self-regulated soft actuators.

Self-regulated heterogeneous hydrogel actuators

We employed a localized actuation method using a focused NIR laser as a primary actuation strategy for soft actuators,[30,37] where the focused laser spot triggers rapid photothermal conversion of the hydrogels, causing localized contraction and bending deformations. As shown in Fig. 3a, we first investigate the design of an up–down type hydrogel actuator (design length: ≈10 mm) with the bottom end fixed to a PDMS base (Fig. S5, ESI†). The hydrogel is immersed in water and driven

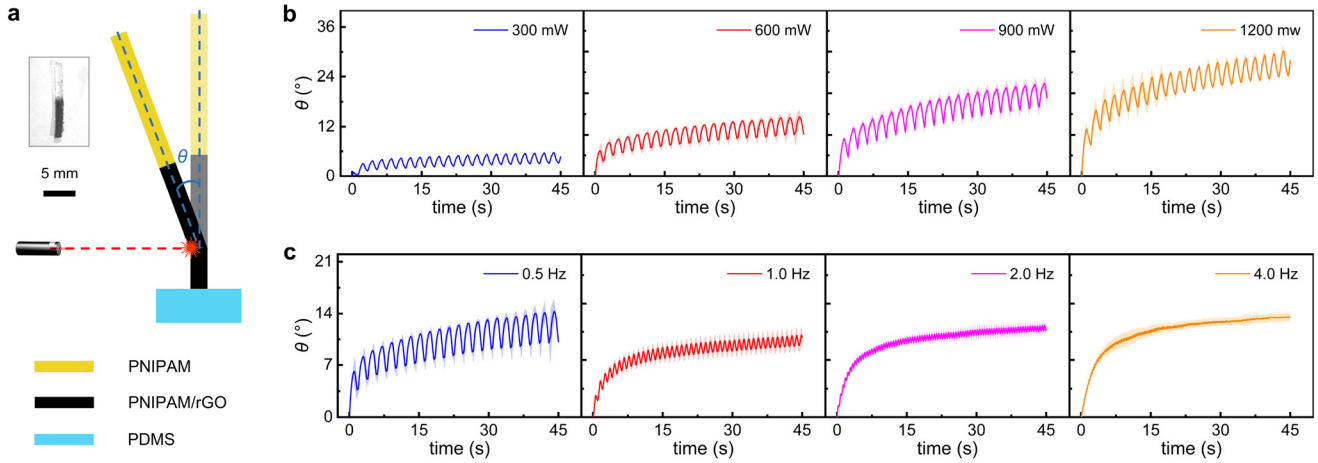

Fig. 3 NIR laser-driven bending and oscillation of up–down-type heterogeneous hydrogel actuators (mean ± SD for two samples, three trials for each sample). (a) Illustration of hydrogel actuator bending. The inset shows the actual image of the swollen actuator, the sizes of which are larger than the designed dimensions due to swelling. (b) On–off light field (frequency: 0.5 Hz)-driven actuator oscillation at different laser intensities. (c) On–off light field (light intensity: 600 mW)-driven actuator oscillation at different frequencies.

using a stationary NIR laser. The diameter of the soft actuator (≈0.9 mm) is sufficient to create a difference in laser intensities between the illuminated side and the shaded side, resulting in localized contraction and bending toward the light source, even within homogeneous PNIPAM/rGO hydrogels. When the light source is turned off, the localized temperature of the hydrogel decreases below its LCST in the aquatic environment, causing water absorption and allowing the hydrogel to swell back to its original shape. We evaluate the hydrogel's ability to reversibly bend and recover *via* the bending angle θ (Fig. 3a). We consider more than one hundred switching cycles under a periodic on–off light field (Fig. 3b and c, Movie S1, ESI†). The periodic oscillation in θ demonstrates excellent repeatability of the hydrogel actuators. Variations in the laser intensity and switching frequency of the on–off light field affect the oscillatory bending behavior. At a constant frequency of 0.5 Hz (which means the laser is on for 1 s and off for 1 s, completing one full cycle every 2 s), higher laser intensity results in greater oscillation amplitudes, indicated by the increased θ (Fig. 3b). Conversely, at a constant laser intensity (600 mW), the median θ remains steady, but faster switching leads to smaller oscillation amplitudes (Fig. 3c). Additionally, we calibrate the oscillation performances of other length ratios of PNIPAM and PNIPAM/rGO hydrogels in this up–down arrangement (Fig. S6, ESI†) and evaluate the influence of the water bath temperature (Fig. S7, ESI†).

Besides the above basic oscillation mode, we observe more complex, multimodal deformations under fixed and continuous laser irradiation in a hybrid heterogeneous hydrogel actuator (consisting of two side-by-side hydrogels with a cross-sectional size ratio of approximately 1 : 1 arranged in an up–down type; cross-section: 1 mm × 1 mm; length: ≈20 mm; Fig. S8, ESI†). We observe a transition of self-regulated deformation modes with increased laser intensity P (Fig. 4). The deformation modes are sequentially named modes 1–4, based on the triggering light intensity, from low to high (Movie S2, ESI†).

Fig. 4a-i depicts mode 1 activated at P = 700 mW, where the actuator exhibits single bending deformation with a bending angle θ_1. With a side-by-side configuration in the illuminated area, the exposed PNIPAM/rGO section rapidly contracts and allows the actuator to reach a steady state at $\theta_1 \approx 82.5°$ (as shown in Fig. 4a-ii and iii). Fig. 4b-i depicts mode 2 activated at P = 1000 mW, where the actuator transitions to single bending deformation with self-regulated oscillation. In this mode, the increased laser intensity causes an increase in θ_1 to ≈85°, which is sufficient for the actuator's top to block the irradiated area near the bottom. This eventually leads to a self-oscillating state under intermittent illumination and self-shadowing (Fig. 4b-ii). This self-regulation behavior is captured by the slight fluctuations in θ_1 around 85° (Fig. 4b-iii). As P increases to 1400 mW, the actuator transitions to mode 3, characterized by self-regulated double bending and oscillation (Fig. 4c-i and ii). Similar to mode 2, sufficient laser intensity triggers a self-oscillating state of the actuator. Yet, the higher laser intensity in mode 3 increases θ_1 to ≈90° (Fig. 4c-iii). This increase in θ_1 causes the PNIPAM/rGO hydrogel layer originally located on the backlight side to move into the illuminated area during the oscillation. As a result, a secondary bending is gradually triggered from 50 s to 200 s and reaches a stable oscillation after 200 s, as shown by the change in θ_2 (Fig. 4c-iii). When P increases to 1500 mW, the actuator transitions to mode 4, characterized by over bending (Fig. 4d-i and ii), and θ_1 reaches ≈100° (Fig. 4d-iii). In this case, the upper hydrogel is no longer illuminated, and thus unable to exhibit secondary bending. Hence, the hybrid heterogeneous configurations enable hydrogel actuators to achieve complex multimodal deformations under fixed NIR laser illumination. Our results demonstrate the intricate relationship between the laser inten-

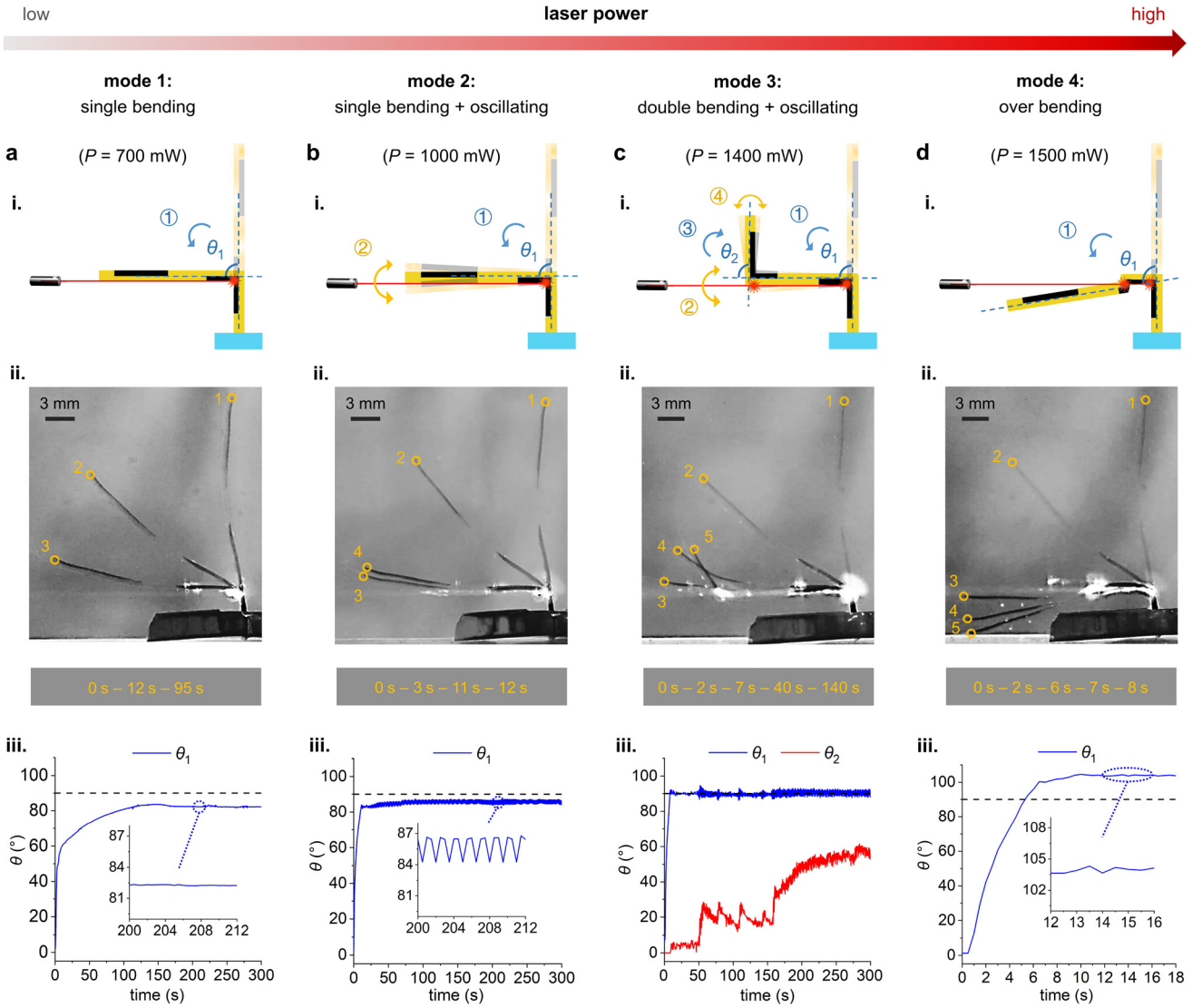

Fig. 4 Self-regulated multimodal deformations of the hydrogel actuator with hybrid heterogeneous configurations under fixed NIR laser actuation. (a) Mode 1: single bending, including (i) illustration; (ii) three experimental snapshots superimposed based on the time sequence; and (iii) variations of θ_1 over time. (b) Mode 2: single bending and oscillation, including (i) illustration; (ii) four experimental snapshots superimposed based on the time sequence; and (iii) variations of θ_1 over time. (c) Mode 3: double bending and oscillation, including (i) illustration; (ii) five experimental snapshots superimposed based on the time sequence; and (iii) variations of θ_1 and θ_2 over time. (d) Mode 4: over bending, including (i) illustration; (ii) five experimental snapshots superimposed based on the time sequence; and (iii) variations of θ_1 over time.

sity and the self-regulated multimodal deformations of the hydrogel actuator (see Fig. S11 and S12, ESI† for further discussions).

Self-regulated hydrogels for complex deformations

Inspired by the self-regulation properties, we propose additional heterogeneous hydrogel designs to showcase their potential for complex deformations under fixed NIR laser actuation, including finger-like bending, and out-of-plane bending resembling the movement of flexible industrial robotic manipulators.

We propose an up–down configuration of two hydrogels arranged side-by-side, as shown in Fig. 5a (type-1 hydrogel actuator; cross section: 1 mm × 1 mm; length: ≈20 mm; Fig. S9, ESI†). In contrast to the arrangement shown in Fig. 4, here we consider PNIPAM/rGO hydrogels in the type-1 actuator positioned on the same side. This hydrogel actuator exhibits double-bending deformation *via* two-step deformation triggered by continuous illumination of two different laser intensities, where the illuminated positions function like finger joints (Fig. 5b and c and Movie S3, ESI†). As an example to illustrate this two-step deformation, we first introduce a continuous laser at 700 mW to the hydrogels for 10 s, which initiates the first bending ① of the soft actuator. Then, we increase the laser intensity to 1100 mW to enhance the bending further, allowing light to reach the upper hydrogel section and creating

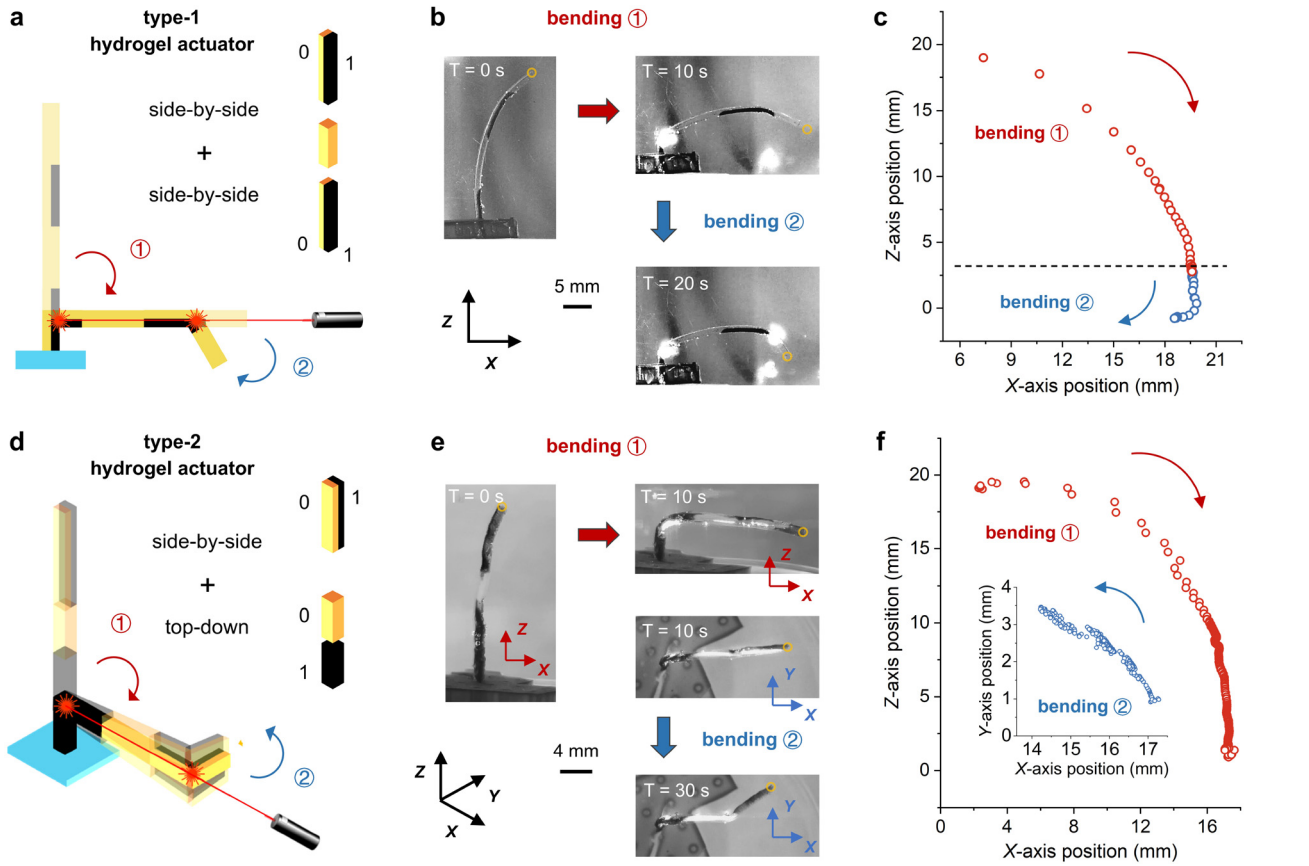

Fig. 5 Heterogeneous hydrogel actuators for self-regulated biomimetic deformations. (a) Illustration of the heterogeneous composition of the type-1 hydrogel actuator. (b) Experimental snapshots showing the finger-like double bending of the type-1 actuator. (c) The motion trajectory of the hydrogel actuator tip during finger-like bending. (d) Illustration of the heterogeneous composition of the type-2 hydrogel actuator. (e) Experimental snapshots depicting the out-of-plane double bending of the type-2 actuator. (f) The motion trajectory of the hydrogel actuator tip during out-of-plane bending.

a secondary bending ② there. In the motion recording, the hydrogel actuator's main axis is defined as the *Z*-axis, and the laser's illumination path is set as the *X*-axis. The motion trajectory of the actuator tip is shown in Fig. 5c using the illuminated point as the origin. In Fig. 5c, the red and blue data points represent bending ① (0–10 s) and bending ② (10–20 s), respectively, along with arrows indicating the bending directions. The type-1 actuator undergoes two instances of clockwise bending, and exhibits an increased tip trajectory curvature due to the second laser exposure point being closer to the top. This results in more complex hydrogel dynamics, leading to multi-joint bending that resembles a finger movement.

An alternative design that features up–down-arranged hydrogels at the bottom and side-by-side-arranged hydrogels at the top is shown in Fig. 5d (type-2 hydrogel actuator; cross-section: 1 mm × 1 mm; length: ≈20 mm; Fig. S10, ESI†). The illuminated homogeneous structure allows for bending in response to laser light from any direction; however, it requires a stronger actuation laser intensity to achieve the initial bending compared to the side-by-side arrangement. Therefore, we set a constant high power of P = 1600 mW to drive the hydrogel actuator's out-of-plane double bending (Movie S4, ESI†). During the first 10 s, the soft actuator performs bending ① in the *XZ*-plane (Fig. 5e and f). When the laser illuminates the upper hydrogel section, it triggers bending ② in the *XY*-plane from 10 s to 30 s (Fig. 5e and f). As defined by the three-dimensional coordinate system shown in Fig. 5d and e, the actuator tip's motion trajectory is shown in Fig. 5f using the illuminated point as the origin. In Fig. 5f, the red and blue data points represent bending ① (0–10 s) and bending ② (10–30 s), respectively, along with arrows indicating the bending directions. The local change of hydrogel dynamics in the upper heterogeneous section enables the type-2 actuator to demonstrate distinct out-of-plane deformation compared to previous hydrogel deformations (Fig. 4 and Fig. 5a–c), resembling flexible industrial manipulators.

The above results further demonstrate how the hybrid-type heterogeneous hydrogels enable self-regulated deformations with versatile actuation modes under a single fixed NIR laser. This advancement is beneficial for developing automated soft robotics with complex dynamics. Most classical methods, whether targeting finger-like bending or in-plane/out-of-plane

multi-bending deformations, often necessitate sophisticated designs and actuation mechanisms, *e.g.*, pneumatic soft actuators with particle jamming,[45] and oscillators with coordinated multiple actuation sources.[38] Here we provide an alternative approach that reduces design complexity and inspires future nature-inspired movements and adaptive systems, promising accessible and versatile robotic solutions that can dynamically respond to their environments.

Conclusions

In this work, we present a new paradigm of self-regulated heterogeneous hydrogel actuators using a single fixed NIR laser for actuation. By coupling heterogeneous designs and a constant light field, we induce self-shadowing and secondary excitation effects in hydrogel actuators. Specifically, the localized shrinkage of the hydrogel actuator causes bending deformation towards the light source, which prompts a shading effect enabling the oscillatory behavior of the actuator. During these oscillations, the hybrid heterogeneous structure triggers secondary bending at higher light intensities. This approach enables self-regulation of the soft actuators, as evidenced by their multimodal deformation in response to varying NIR laser intensities (Fig. 4). Additionally, to validate the generality and scalability of this concept, we examine various types of actuators that can simulate in-plane finger-like bending and out-of-plane manipulator-like bending under the fixed NIR laser arrangement (Fig. 5). In the next phase, we will focus on the comprehensive optimization of hydrogel actuators, which includes enhancing material performance, refining design parameters, developing theoretical models, and exploring practical applications. Moreover, future research on developing untethered actuators by using a similar heterogeneous design concept, along with alternative actuation mechanisms (*e.g.*, magnetic fields[46,47]) or in different environments (*e.g.*, airborne[48]), may enhance the autonomy and adaptive behavior of innovative self-regulated actuators, and ultimately transform applications in robotics, automation, and biomedical fields.

Experimental section

Materials

N-Isopropylacrylamide (≥98%), *N*,*N*′-methylenebisacrylamide (BIS) (≥99%), 2-hydroxy-2-methylpropiophenone (≥97%), acrylamide (≥99%), and ascorbic acid (≥99%) were obtained from Aladdin Industrial Co., Ltd (China). Graphene oxide aqueous solution (concentration: 5 mg mL^{-1}; thickness: 0.6–1 nm; flake diameter: 0.5–5 μm) was provided by Tanfeng Graphene Technology Co., Ltd (China). Sylgard 184 polydimethylsiloxane (PDMS) and its curing agent were obtained from Dow Corning Co. (USA). Deionized (DI) water was produced by the Direct-Q deionized water system (USA). All chemicals were used as received.

Preparation of PNIPAM and PNIPAM/rGO hydrogels

The PNIPAM precursor was prepared by mixing *N*-isopropylacrylamide, acrylamide, BIS, 2-hydroxy-2-methylpropiophenone, and DI water in a mass ratio of 120 : 24 : 3 : 8 : 100. For the PNIPAM/GO precursor, the same mass ratio was maintained, and graphene oxide aqueous solution was added to achieve specific photothermal agent concentrations (0.5, 1, 1.5, and 2.0 mg mL^{-1}). All the precursors were stirred overnight at 200 rpm, then labeled and stored away from light. PNIPAM-based hydrogels were fabricated by exposing the top and bottom sides for ≈15 s under UV light (365 nm, 300 mW cm^{-2}). In the heterogeneous design, light-curing assembly and layer-by-layer exposure were aided by molds (Fig. S5 and S8–S10†). After cross-linking, the PNIPAM/GO hydrogel was immersed in a 0.1 g mL^{-1} ascorbic acid aqueous solution to reduce GO in the hydrogel matrix, followed by heating in a 90 °C water bath for 1 hour. The samples were then soaked in DI water (25 °C) until the swelling equilibrium was reached for later use. We observed that slight variations in the ratio of the two heterogeneous portions (PNIPAM and PNIPAM/rGO) and the size/concentration of rGO do not significantly affect the overall deformation modes of the soft actuators.

Microscopy

The SEM images were obtained using a Hitachi S-4800 scanning electron microscope. Experiments were performed using a handheld microscope (Dino-Lite Edge AM4115ZTL, AnMo, Taiwan).

FTIR spectroscopy

The data were obtained using a Nicolet iS50 FTIR spectrometer (Thermo Scientific). The disk-shaped samples (diameter: 6 mm; thickness: 3 mm) were dried at 80 °C for 24 hours before tests.

Tensile strength test

The mechanical properties of the hydrogels were tested using dynamic mechanical analysis (DMA) with DMA Q800 V21.2 Build 88 apparatus (TA Instruments, USA). The samples were rod-shaped hydrogels (diameter: 1 mm; length: 20 mm), soaked in DI water at 25 °C for 48 hours to reach the swelling equilibrium before testing.

Swelling property characterization

First, we measured the dry weight of the hydrogel as M_0 and its volume as V_0. Then, the hydrogel sample was placed in DI water at 25 °C for 48 hours to reach the swelling equilibrium before removing them. After that, we used absorbent paper to dry the surface moisture, and recorded its weight M_1 and volume V_1. Finally, the R_M and R_V values could be acquired using the following equations:

$$R_M = (M_1 - M_0)/M_1 \times 100\% \quad (1)$$

$$R_V = (V_1 - V_0)/V_1 \times 100\% \quad (2)$$

Laser system and photothermal response test

The photothermal response was induced using an 808 nm NIR laser source (TZ808AD2000-F100-GQ, Shenzhen Taizhu Technology), which was modulated using a function generator (Topward, 8150). The NIR laser used is equipped with a collimator and features focal length adjustment, allowing for precise control of the laser beam diameter during actuator driving experiments. Within a range of approximately 1 meter, the beam diameter can be adjusted to 2–3 mm by modifying the focal length, facilitating the actuation of various hydrogel samples. For the photothermal response tests, the disk-shaped samples (diameter: 6 mm; thickness: 3 mm) were soaked in DI water (25 °C) for 48 hours until the swelling equilibrium was reached, and then removed from the water for testing. The NIR laser was adjusted to focus the spot on the center of the sample, and the output power was modified on demand. Thermal images of the samples under laser irradiation (Fig. 2e) were captured using a thermal imager (HM-TPK20-3AQF/W, Hikvision) to record temperature changes over time at the same irradiation duration, assessing the photothermal response performance of the hydrogels with different photothermal agent concentrations (Fig. S2 and S3, ESI†).

Viscosity measurement of the precursors

Fig. S4 (ESI)† shows the viscosity of the hydrogel precursors used in this study, measured using a digital viscometer (range: 0.1–100 000 mPa s; resolution: ±2%; SNB-2, AOYIMEI, China).

PDMS substrate/mold preparation

In this study, PDMS molds and PDMS substrates were used for the fabrication of hydrogel actuators. Different-shaped PDMS molds/substrates were fabricated through a molding process. Specifically, PDMS and the curing agent were mixed in a mass ratio of 10 : 1, thoroughly stirred, and degassed for 1 hour. The mixture was then poured into the mold and heated in an oven at 70 °C for 2 hours. Finally, the sample was obtained by demolding.

Data acquisition

The quantitative data of deformations were collected by using Tracker software video analysis.

Author contributions

J. L., J. M. and A. C. H. T. conceived this study. J. M. and A. C. H. T. supervised the project. J. L. and J. M. carried out the experiments. A. C. H. T. acquired funding. J. L., J. M. and A. C. H. T. contributed to the interpretation of the results. J. L., J. M. and A. C. H. T. drafted and revised the manuscript.

Data availability

All data supporting the conclusions in this paper are presented in the main text and the ESI.† Additional data related to this paper may be requested from the authors.

Conflicts of interest

There are no conflicts to declare.

Acknowledgements

The authors are grateful for funding support from the Croucher Foundation and for equipment support from the HKU Queen Mary Hospital Electron Microscope Unit.

References

1 M. Ilami, H. Bagheri, R. Ahmed, E. O. Skowronek and H. Marvi, *Adv. Mater.*, 2021, **33**, 2003139.
2 M. Li, A. Pal, A. Aghakhani, A. Pena-Francesch and M. Sitti, *Nat. Rev. Mater.*, 2022, **7**, 235–249.
3 J. Miao and S. Sun, *J. Magn. Magn. Mater.*, 2023, **586**, 171160.
4 Z. Xie, F. Yuan, J. Liu, L. Tian, B. Chen, Z. Fu, S. Mao, T. Jin, Y. Wang, X. He, *et al.*, *Sci. Rob.*, 2023, **8**, eadh7852.
5 H. Niu, R. Feng, Y. Xie, B. Jiang, Y. Sheng, Y. Yu, H. Baoyin and X. Zeng, *Soft Rob.*, 2021, **8**, 507–518.
6 Y. Wang, X. Du, H. Zhang, Q. Zou, J. Law and J. Yu, *Adv. Sci.*, 2023, **10**, 2207493.
7 R. F. Shepherd, F. Ilievski, W. Choi, S. A. Morin, A. A. Stokes, A. D. Mazzeo, X. Chen, M. Wang and G. M. Whitesides, *Proc. Natl. Acad. Sci. U. S. A.*, 2011, **108**, 20400–20403.
8 W. Hu, G. Z. Lum, M. Mastrangeli and M. Sitti, *Nature*, 2018, **554**, 81–85.
9 J. Miao, T. Zhang, G. Li, D. Guo, S. Sun, R. Tan, J. Shi and Y. Shen, *Engineering*, 2023, **23**, 170–180.
10 L. C. van Laake and J. T. B. Overvelde, *Commun. Mater.*, 2024, **5**, 198.
11 K. Kwan, S. Li, N. Hau, W.-D. Li, S. Feng and A. H. Ngan, *Sci. Rob.*, 2018, **3**, eaat4051.
12 X. Fan, Y. Zhang, Z. Wu, H. Xie, L. Sun, T. Chen and Z. Yang, *Nanoscale*, 2023, **15**, 19499–19513.
13 R. Yun, J. Che, Z. Liu, X. Yan and M. Qi, *Nanoscale*, 2023, **15**, 12933–12943.
14 C. S. X. Ng, M. W. M. Tan, C. Xu, Z. Yang, P. S. Lee and G. Z. Lum, *Adv. Mater.*, 2021, **33**, 2003558.
15 J. Li, J. Deng, S. Zhang, W. Chen, J. Zhao and Y. Liu, *Adv. Sci.*, 2023, **10**, 2305128.
16 M. Cianchetti, C. Laschi, A. Menciassi and P. Dario, *Nat. Rev. Mater.*, 2018, **3**, 143–153.
17 C. Wang, Y. Wu, X. Dong, M. Armacki and M. Sitti, *Sci. Adv.*, 2023, **9**, eadg3988.

18 R. Tan, X. Yang, H. Lu, L. Yang, T. Zhang, J. Miao, Y. Feng and Y. Shen, *Matter*, 2022, **5**, 1277–1295.
19 J. Liu, L. Jiang, S. He, J. Zhang and W. Shao, *Chem. Eng. J.*, 2022, **433**, 133496.
20 J. Jiang, S. Xu, H. Ma, C. Li and Z. Huang, *Mater. Today Bio*, 2023, **20**, 100657.
21 X. Peng, C. Jiao, Y. Zhao, N. Chen, Y. Wu, T. Liu and H. Wang, *ACS Appl. Nano Mater.*, 2018, **1**, 1522–1530.
22 D. Kim, H. S. Lee and J. Yoon, *Sci. Rep.*, 2016, **6**, 20921.
23 Z. J. Wang, C. Y. Li, X. Y. Zhao, Z. L. Wu and Q. Zheng, *J. Mater. Chem. B*, 2019, **7**, 1674–1678.
24 X. Wei, Y. Xue, Y. Sun, L. Chen, C. Zhang, Q. Wu, S. Peng, C. Ma, Z. Liu, S. Jiang, *et al.*, *Chem. Eng. J.*, 2023, **452**, 139373.
25 C. Yin, F. Wei, S. Fu, Z. Zhai, Z. Ge, L. Yao, M. Jiang and M. Liu, *ACS Appl. Mater. Interfaces*, 2021, **13**, 47147–47154.
26 L. Tang, L. Wang, X. Yang, Y. Feng, Y. Li and W. Feng, *Prog. Mater. Sci.*, 2021, **115**, 100702.
27 H. Fu, K. Xue, Y. Zhang, M. Xiao, K. Wu, L. Shi and C. Zhu, *Adv. Sci.*, 2023, **10**, 2206865.
28 R. B. Yilmaz, Y. Chaabane and V. Mansard, *ACS Appl. Mater. Interfaces*, 2023, **15**, 7340–7352.
29 W. Yang, Q. Guo, X. Teng, Z. Qiao and H. Yu, *Sens. Actuators, A*, 2024, **373**, 115437.
30 C. Qian, Y. Li, L. Liu, C. Chen and L. Han, *J. Mater. Chem. C*, 2023, **11**, 6741–6749.
31 G. Hou, X. Zhang, F. Du, Y. Wu, X. Zhang, Z. Lei, W. Lu, F. Zhang, G. Yang, H. Wang, *et al.*, *Nat. Nanotechnol.*, 2024, **19**, 77–84.
32 J. Miao, S. Sun, T. Zhang, G. Li, H. Ren and Y. Shen, *ACS Appl. Mater. Interfaces*, 2022, **14**, 50296–50307.
33 D. Martella, S. Nocentini, C. Parmeggiani and D. S. Wiersma, *Adv. Mater. Technol.*, 2019, **4**, 1800571.
34 Q. L. Zhu, W. Liu, O. Khoruzhenko, J. Breu, W. Hong, Q. Zheng and Z. L. Wu, *Nat. Commun.*, 2024, **15**, 300.
35 J. Miao, *Sens. Actuators, A*, 2024, **368**, 115104.
36 S. Li, M. M. Lerch, J. T. Waters, B. Deng, R. S. Martens, Y. Yao, D. Y. Kim, K. Bertoldi, A. Grinthal, A. C. Balazs, *et al.*, *Nature*, 2022, **605**, 76–83.
37 Y. Zhao, C. Xuan, X. Qian, Y. Alsaid, M. Hua, L. Jin and X. He, *Sci. Rob.*, 2019, **4**, eaax7112.
38 Z. Deng, H. Zhang, A. Priimagi and H. Zeng, *Adv. Mater.*, 2024, **36**, 2209683.
39 D. Wu, X. Li, Y. Zhang, X. Cheng, Z. Long, L. Ren, X. Xia, Q. Wang, J. Li, P. Lv, *et al.*, *Adv. Sci.*, 2024, **11**, 2400557.
40 M. Li, A. Pal, A. Aghakhani, A. Pena-Francesch and M. Sitti, *Nat. Rev. Mater.*, 2022, **7**, 235–249.
41 J. Miao and A. C. Tsang, *Adv. Sci.*, 2024, **11**, 2405641.
42 X. Cui, Y. Zeng, L. Qin, X. Cheng and Y. Yang, *Adv. Mater. Technol.*, 2024, **9**, 2302099.
43 D. Li, X. Zhang, J. Yao, G. P. Simon and H. Wang, *Chem. Commun.*, 2011, **47**, 1710–1712.
44 M. A. Haq, Y. Su and D. Wang, *Mater. Sci. Eng., C*, 2017, **70**, 842–855.
45 Y. Li, Y. Chen, Y. Yang and Y. Wei, *IEEE Trans. Rob.*, 2017, **33**, 446–455.
46 L. Yang, J. Miao, G. Li, H. Ren, T. Zhang, D. Guo, Y. Tang, W. Shang and Y. Shen, *ACS Appl. Polym. Mater.*, 2022, **4**, 5431–5440.
47 M. Ha, H. Kwon, Y. Yang, G. Kim and D. Gim, *Nanoscale*, 2024, **16**, 6778–6819.
48 Y. Zhao, Z. Liu, P. Shi, C. Chen, Y. Alsaid, Y. Yan and X. He, *Nat. Mater.*, 2025, **24**, 116–124.